Finite-size effects of hysteretic dynamics in multilayer graphene on a ferroelectric

Anna N. Morozovska,[1] Anastasiia S. Pusenkova,[2] Oleksandr V. Varenyk,[1] Sergei V. Kalinin,[3]
Eugene A. Eliseev,[4] and Maxym V. Strikha[5,*]

[1]*Institute of Physics, National Academy of Sciences of Ukraine, Kyiv, Ukraine*
[2]*Taras Shevchenko Kyiv National University, Physics Faculty, Kyiv, Ukraine*
[3]*The Center for Nanophase Materials Sciences and Materials Science and Technology Division, Oak Ridge National Laboratory, Oak Ridge, Tennessee 37831, USA*
[4]*Institute for Problems of Material Sciences, National Academy of Sciences of Ukraine, Kyiv, Ukraine*
[5]*V. E. Lashkarev Institute of Semiconductor Physics, National Academy of Sciences of Ukraine, Kyiv, Ukraine*

(Received 14 December 2014; revised manuscript received 10 April 2015; published 11 June 2015)

The origin and influence of finite-size effects on the nonlinear dynamics of space charge stored by multilayer graphene on a ferroelectric and resistivity of graphene channel were analyzed. Here, we develop a self-consistent approach combining the solution of electrostatic problems with the nonlinear Landau-Khalatnikov equations for a ferroelectric. The size-dependent behaviors are governed by the relations between the thicknesses of multilayer graphene, ferroelectric film, and the dielectric layer. The appearance of charge and electroresistance hysteresis loops and their versatility stem from the interplay of polarization reversal dynamics and its incomplete screening in an alternating electric field. These features are mostly determined by the dielectric layer thickness. The derived analytical expressions for electric fields and space-charge-density distribution in a multilayer system enable knowledge-driven design of graphene-on-ferroelectric heterostructures with advanced performance. We further investigate the effects of spatially nonuniform ferroelectric domain structures on the graphene layers' conductivity and predict its dramatic increase under the transition from multi- to single-domain state in a ferroelectric. This intriguing effect can open possibilities for the graphene-based sensors and explore the underlying physical mechanisms in the operation of graphene field-effect transistor with ferroelectric gating.

DOI: 10.1103/PhysRevB.91.235312 PACS number(s): 72.80.Vp, 77.84.Ek, 77.80.bn

I. INTRODUCTION

The seminal works by Geim and Novoselov [1–3] have become the harbinger of the new area of graphene physics at the junction between condensed matter and surface physics and physical chemistry. In the initial wave of graphene research, the attention of the scientific community has been primarily focused on the properties of graphene *per se*. However, it has been rapidly realized that many unique functionalities of graphene are strongly affected by interaction with substrate, gates, contacts, thermostat, and surface and interface adsorbates [4,5].

Particularly of interest are the studies of graphene on the substrates with high permittivity, since these allow to achieve a higher carrier concentration for the same gate voltages [5–7]. In particular, using ferroelectrics instead of traditional high-k substrates offers dual advantages of high dielectric constant and nonvolatile memory effects via polarization switching [8–15]. Here, the charge carriers in graphene screen the depolarization electric field induced by discontinuity of spontaneous polarization at the ferroelectric surface [16–18], allowing for dynamic control of carrier concentration in graphene. The first study focused on a graphene-on-ferroelectric device appeared in 2009 [8], and the number of such works has increased, and several reviews have already been published (see, e.g., [19–21]).

Notably, hysteretic ferroelectric gating and symmetrical bit writing in graphene-ferroelectric field-effect transistors (GFeFETs) with an electroresistance change of over 500% and a reproducible, nonvolatile switching have been demonstrated [10]. However, a comprehensive understanding of the nonlinear, hysteretic ferroelectric gating in GFeFETs is still absent [10]. This motivates us to develop the continuum media theory of the size effects influenced on the stored charge and electroresistance nonlinear hysteretic dynamics in the multilayer graphene on ferroelectric.

Below we present the modified continuum media approach, which combines the solution of the electrostatic problem with the nonlinear Landau-Khalatnikov equation in a self-consistent way in order to describe analytically the nonlinear dynamics of the ferroelectric polarization reversal. We note that the continuum media approach is nonapplicable to a monolayer graphene and partially applicable to ultrathin graphite layers. However, the approach has the unique advantage of yielding universal analytical expressions in terms of specific material parameters. As such, it can be directly matched to experiment. Here, we consider dynamic hysteretic effects in graphene layers of finite thickness extending thermodynamic studies [17], obtain analytical expressions for electric fields and space-charge-density distribution in a multilayer system, and establish the impact of a buffer dielectric layer between graphene and ferroelectric surface in the multidomain state. The analytical results allow a comprehensive understanding of the physical process, and also allow to predict and to analyze multiscale size effects in the system, which opens an effective way to control and optimize its nonlinear and hysteretic properties.

II. PROBLEM STATEMENT

Geometry of the considered GFeFET with two gates (similar geometry was used in Refs. [8,10]) is shown in Fig. 1. Multilayered graphene (MLG) of thickness d has a background permittivity ε_G. The ultrathin dielectric layer has

*Corresponding author: maksym_strikha@hotmail.com

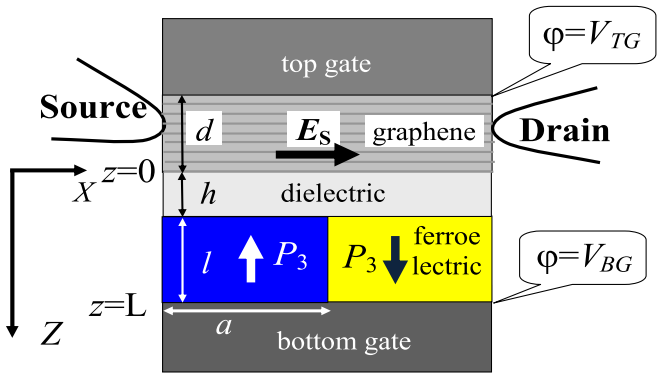

FIG. 1. (Color online) Geometry of the FET heterostructure. Shown are the top gate, MLG, dielectric layer, ferroelectric, and bottom gate arranged vertically, as well as lateral source and drain electrodes.

thickness h and dielectric permittivity ε_d. We note that this imposes limits on h, which should be at least several lattice constants or higher, because permittivity ε_d trends to zero for the smaller h. A ferroelectric film with 180° domain structure and spontaneous polarization vector $\mathbf{P}_S = (0,0,P_3)$ has thickness l. The period of 180° domain structure is a. The ac voltage V_{TG} is applied to the top gate electrode, whereas dc voltage V_{BG} is applied to the bottom gate electrode. The gate voltages determine the Fermi energy level E_F position in graphene and hence local electron concentration. Furthermore, the driving field E_S is applied across the MLG channel.

The system of electrostatic equations for the graphene layer ($-d < z < 0$), dielectric layer ($0 < z < h$), and ferroelectric ($h < z < L$) layers are

$$\Delta\varphi_G - \frac{\varphi_G}{R_t^2} = 0\Big|_{-d<z<0}, \quad \Delta\varphi_d = 0|_{0<z<h},$$
$$\varepsilon_{33}^f \frac{\partial^2\varphi_f}{\partial z^2} + \varepsilon_{11}^f\left(\frac{\partial^2\varphi_f}{\partial x^2} + \frac{\partial^2\varphi_f}{\partial y^2}\right) = 0\Big|_{h<z<L}. \tag{1}$$

Here, Δ is the Laplace operator. Thickness $L = l + h$ and ε_{ij}^f are the linear dielectric permittivity tensor components; R_t is a screening radius [22]. The latter can be estimated using Debye or Thomas-Fermi approximations depending on the electronic properties of the heterostructure.

Equation (1) is supplemented by the boundary conditions for the electric potential φ and continuity of the normal component of electric displacement $\mathbf{D}$ at the interfaces $z = -d$, $z = 0$, $z = h$, and $z = L$. Displacement is related to ferroelectric polarization as $D_3^f = \varepsilon_0\varepsilon_{33}^f E_3^f + P_3$. $D_3^d = \varepsilon_0\varepsilon^d E_3^d$ in the dielectric layer and $D_3^G = \varepsilon_0\varepsilon^G E_3^G$ in the graphene ($\varepsilon_0 = 8.85\times10^{-12}$ F/m is the universal dielectric constant). When an electric current along the graphene channel is absent ($E_S = 0$), but nonzero top and bottom gate voltages are applied, they acquire the following form:

$$\begin{aligned}\varphi_G(x,y,-d) &= V_{TG},\\ \varphi_G(x,y,0) &= \varphi_d(x,y,0),\\ \varphi_d(x,y,h) &= \varphi_f(x,y,h),\\ \varphi_f(x,y,L) &= V_{BG},\end{aligned} \tag{2a}$$
$$-\varepsilon_G\frac{\partial\varphi_G}{\partial z} + \varepsilon_d\frac{\partial\varphi_d}{\partial z}\Big|_{z=0} = 0,$$
$$-\varepsilon_{33}^f\frac{\partial\varphi_f}{\partial z} + P_3 + \varepsilon_d\frac{\partial\varphi_d}{\partial z}\Big|_{z=h} = 0, \tag{2b}$$

In ferroelectric, the polarization is given by the time-dependent Landau-Khalatnikov (LK) equation that states

$$\Gamma\frac{\partial}{\partial t}P_3 + \alpha P_3 + \beta P_3^3 + \gamma P_3^5 - g\Delta P_3 = E_3^f, \tag{3}$$

supplemented by the natural boundary conditions, $(\partial P_3/\partial z)|_{z=h,L} = 0$.

III. ANALYTICAL SOLUTION FOR A SINGLE-DOMAIN STATE OF FERROELECTRIC

Analytical expressions for the electric potential inside each layer are listed in the Appendix. The electric field in the ferroelectric is the sum of depolarization and external components:

$$E_3^f = E_3^d + E_3^{\text{ext}}, \tag{4a}$$
$$E_3^{\text{ext}} = \frac{\varepsilon_d\varepsilon_G[2V_{TG}e^{d/R_t} - V_{BG}(e^{2d/R_t}+1)]}{\varepsilon_d\varepsilon_G l(e^{2d/R_t}+1) + \varepsilon_{33}^f[\varepsilon_G h(e^{2d/R_t}+1) + \varepsilon_d R_t(e^{2d/R_t}-1)]}, \tag{4b}$$
$$E_3^d = \frac{-[\varepsilon_G h(e^{2d/R_t}+1) + \varepsilon_d R_t(e^{2d/R_t}-1)](P_3/\varepsilon_0)}{\varepsilon_d\varepsilon_G l(e^{2d/R_t}+1) + \varepsilon_{33}^f[\varepsilon_G h(e^{2d/R_t}+1) + \varepsilon_d R_t(e^{2d/R_t}-1)]}. \tag{4c}$$

The field is constant in the z direction and depends on the screening radius R_t and polarization P_3. The latter depends on R_t via the electric field inside the ferroelectric layer, hence yielding a coupled problem. The depolarization field leads to the film ferroelectric properties degradation with decrease in l and to the ferroelectricity disappearance at l less than the critical value $l < l_{cr}$. The critical thickness l_{cr} depends on h, d, R_t, and dielectric permittivities ε_G, ε_d, and ε_{33}^f, as well as on the ferroelectric material parameter α. At fixed l value the increase of h leads to a strong increase of the depolarization field and then to its saturation value, since $E_3^d \approx \frac{C_1h+C_2}{C_3h+C_4}$.

Since the electric field is constant in ferroelectric for the single-domain case, the solution of the LK equation of state (3) becomes consistent with the natural boundary conditions and can be obtained self-consistently from the differential (or algebraic

TABLE I. Range of parameters used in calculations.

Parameters	Value
Screening radius R_t	(0.3-3) nm
Graphite permittivity ε_G	15
Graphene thickness d	(3–30) nm
Residual concentration $n_{\rm res}$	(Varies from 10^{17} to 10^{15} m^{-2}, as the latter value was used in Ref. [10])
Dielectric permittivity ε_d	1 (air); 5–7 (background constant), 12.53 (sapphire Al_2O_3)
Dielectric layer thickness h	(0–50) nm
Dielectric anisotropy of ferroelectric γ	0.58 ($LiNbO_3$); 3.87 (Rochelle salt)
Ferroelectric permittivity ε_{33}^f	29 ($LiNbO_3$); 300 (Rochelle salt)
Ferroelectric polarization P_S	0.75 C/m^2 ($LiNbO_3$); 0.002 C/m^2 (Rochelle salt or relaxor)
LGD parameters for $LiNbO_3$	$\alpha = -1.95\times10^9$ m/F, $\beta = 3.61\times10^9$ $m^5/(C^2F)$, $\gamma = 0$
Ferroelectric thickness l	(10–30) nm
Period of domain structure a	(50–500) nm
Coercive field range	$(2-7)\times10^8$ V/m ($LiNbO_3$); 30 kV/cm (Rochelle salt)

in the stationary case) equation. The total surface charge σ_G stored in graphene is

$$\sigma_G = \frac{\varepsilon_0\varepsilon_d\varepsilon_G\left\{2\varepsilon_{33}^f V_{TG}e^{d/R_t} - \left[\varepsilon_{33}^f V_{BG} - (P_3 l/\varepsilon_0)\right](e^{2d/R_t}+1)\right\}}{\varepsilon_d\varepsilon_G l(e^{2d/R_t}+1) + \varepsilon_{33}^f[\varepsilon_G h(e^{2d/R_t}+1) + \varepsilon_d R_t(e^{2d/R_t}-1)]}. \quad (5)$$

Note that the Eqs. (3) and (4) are coupled, and their self-consistent solution for polarization should be substituted in Eq. (5) to calculate the total charge of graphene. Then the effective surface density of carriers in graphene can be found as $n = -(\sigma_G/e)$ [3], where $e = 1.6\times10^{-19}$ C is the electron charge. Finally, the graphene "effective" electroresistance R can be estimated (see, e.g., [10,14]) as

$$R = \frac{R_0}{\sqrt{1 + n^2/n_{\rm res}^2}}. \quad (6)$$

Here $R_0 = \frac{L_{SD}}{We\mu_{\rm Hall}n_{\rm res}}$, where L_{SD} is the graphene channel length from the source to the drain, W is its width, and $n_{\rm res}$ is a the density of the residual carriers in graphene.

IV. NONLINEAR HYSTERETIC EFFECT ON THE GRAPHENE CONDUCTIVITY AND ELECTRORESISTANCE

In this section we analyze the finite-size effects on the nonlinear dynamics of the space charge in a multilayer graphene when the ferroelectric substrate is in a single-domain case. In particular we study the dependence of P_3, σ_G, and R voltage response on ferroelectric substrate thickness l, dielectric layer thickness h, graphene thickness d, and screening radius R_t. Note that the field does not depend on MLG thickness d separately, but depends on the ratio $2d/R_t$. Following the experimentally adopted configuration [8], here we assume that the bottom gate voltage is constant and the top gate voltage varies with the frequency ω, i.e., $V_{TG} = V_{TG}\sin(\omega t)$. Dimensionless frequency is introduced as $w = -\omega\Gamma/\alpha$. The full set of parameters is listed in Table I.

Nonlinear and hysteresis effects manifest when the electric field in ferroelectric E_3^f is enough to reverse or significantly change its polarization P_3 in agreement with Eq. (3). The polarization hysteresis immediately causes the hysteretic response of the total charge stored in multilayer graphene and its resistance. The heterostructure response can be asymmetric, since the initial direction of polarization breaks the inversion symmetry. Generally these results correspond to the mechanism of the "direct" hysteresis in the graphene channel resistivity, caused by the repolarization of the substrate dipoles (see, e.g., [23]).

Figure 2 shows the ferroelectric polarization P_3, the effective density of the total charge stored in graphene n, and its electroresistance R as a function of the top gate voltages V_{TG} for several values of graphene thickness d. At low frequencies, polarization and charge loops become very slim, strongly tilted and shifted from the coordinate origin with the thickness d decrease. At higher frequencies polarization and total charge loops acquire quasielliptic shape with a noticeable vertical and horizontal asymmetry. Remarkably, the loops' asymmetry increases with d increase, while resistance loops' double shape transforms into a single one for the higher values of d. This strong influence of the heterostructure voltage response on graphene thickness d partially comes from the complex exponential dependence of the depolarization field on the parameter (curves 1–4 in Fig. 2).

The graphene charge loop shape, and the remanent charge and coercive voltage values strongly correlate with the polarization loop, since the charge is proportional to P_3 and V_{BG} in accordance with Eq. (5), namely, $\sigma_G = C_1V_{TG} + C_2V_{BG} + C_3P_3$. Moreover, V_{BG} induces nontrivial vertical and horizontal asymmetry of all the loops. The electroresistance response is defined by the residual carrier density in the graphene, $n_{\rm res}$, and is modulated by an order of magnitude for chosen parameters. It strongly increases with the decrease of $n_{\rm res}$ in agreement with Eq. (6).

The resistance loop shapes shown in Fig. 2(f) are very similar to the experimental ones obtained by Zheng *et al.* (Fig. 2 in Ref. [10]), while the amplitude of ac voltage applied

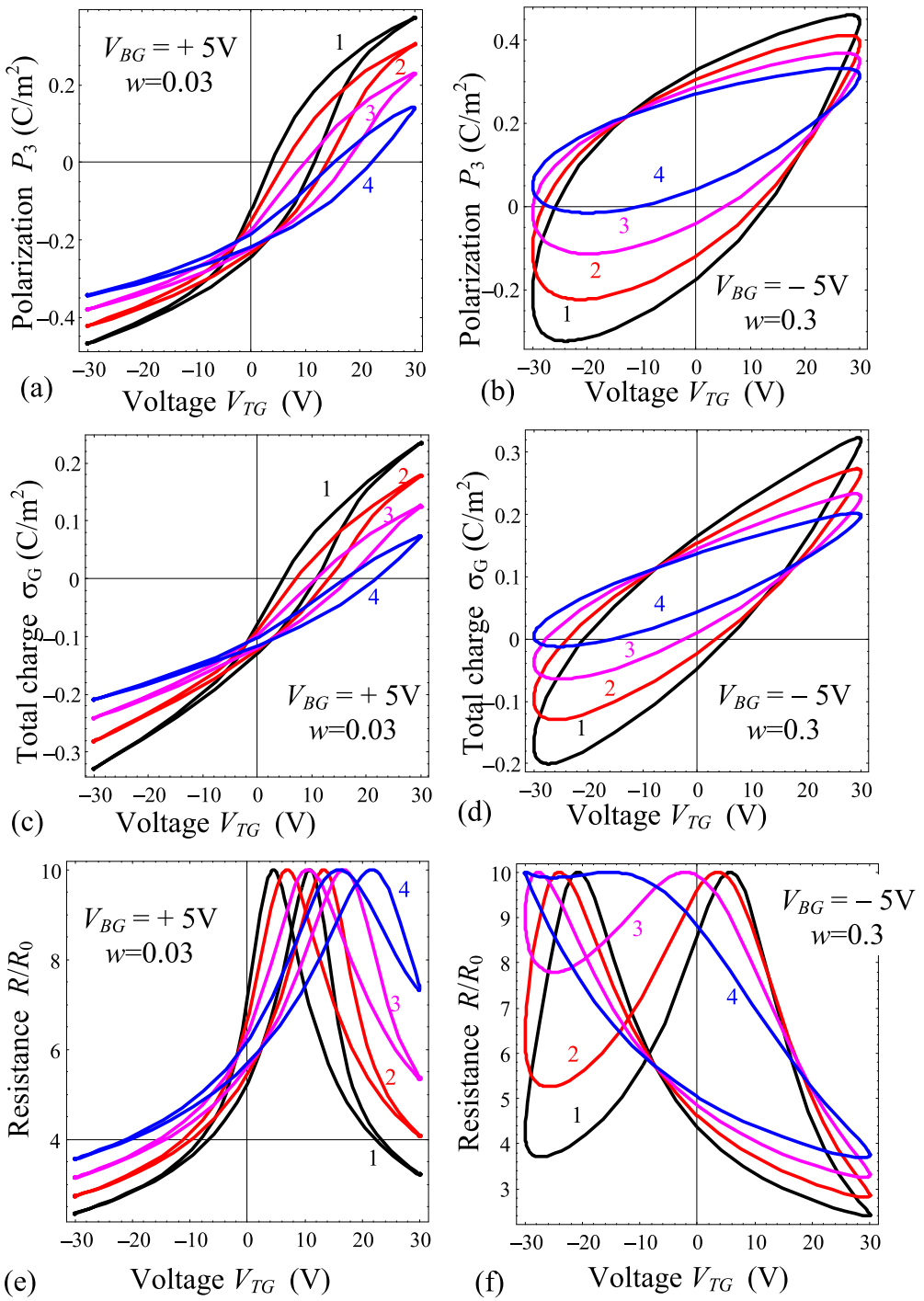

FIG. 2. (Color online) Influence of multilayer graphene thickness. Hysteresis loops of $LiNbO_3$ ferroelectric polarization (a), (b), density of the total charge stored in multilayer graphene (c), (d) and its electroresistance (e), (f) calculated for different thickness of multilayer graphene $d = 3, 4, 5, 6$ nm (curves 1, 2, 3, 4). The frequency $w = 0.03$ and back gate voltage $V_{BG} = +5$ V for plots (a), (c), and (e) (left column); $w = 0.3$ and back gate voltage $V_{BG} = -5$ V for plots (b), (d), and (f) (right column). Sapphire dielectric thickness $h = 10$ nm, screening radius $R_t = 3$ nm, $n_{\text{res}} = 5\times10^{17}$ m^{-2}, ferroelectric film thickness $l = 20$ nm.

to the top gate ($V_{TG0} = 30$ V) was taken much higher than the bottom gate voltage ($V_{BG} = \pm5$ V). Note that analytical results illustrated by Fig. 2 are complementary to the experiment and modeling performed by Zheng *et al.* [10], because we analyzed the influence of the heterostructure finite sizes on graphene sheet conductivity and resistance. Nevertheless the comparison of hysteresis loop shape observed experimentally for graphene field-effect transistors with ferroelectric gating at different back gate voltages [10] with the loop shape calculated theoretically for different thickness of multilayer graphene demonstrates a surprising agreement (compare Fig. 2(f) with Fig. 2 in Ref. [10]).

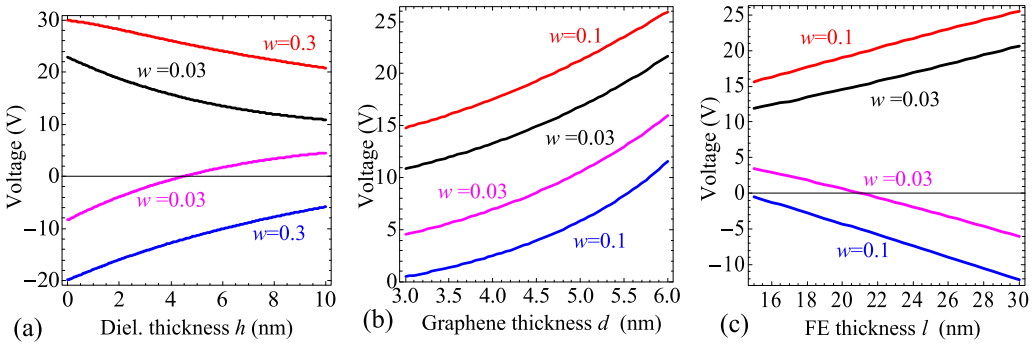

FIG. 3. (Color online) Size effect of coercive voltages. Graphene total charge left and right coercive voltages dependence on the dielectric layer, graphene, and ferroelectric film thicknesses h, d, and l correspondingly calculated for different frequencies $w = 0.01-0.3$ (labels near the curves). Plots (a)–(c) are calculated with the back gate voltage 5 V. For plots (a) $d = 3$ nm, $l = 20$ nm; (b) $h = 10$ nm, $l = 20$ nm; (c) $h = 5$ nm, $d = 3$ nm. Other parameters are the same as in Fig. 2.

Figure 3 illustrates the dependence of the coercive voltages of graphene charge loop on the thicknesses of dielectric layer, graphene, and ferroelectric film for different frequencies w and positive back gate voltage V_{BG}. Positive and negative coercive voltages are equal for the case of $V_{BG} = 0$ and different for nonzero V_{BG}. The coercive voltage decreases with h increase and fixed d and l values. At fixed h the voltage almost linearly increases with d increase or l increase.

Figure 4 shows the dependence of the differential electroresistance, $\delta R = (R_{\max} - R_{\min})/R_{\min}$, on the thickness of the dielectric layer, multilayer graphene, and ferroelectric film for different frequencies w and fixed back gate $V_{BG} = 5$ V. Dependence of δR on h has a pronounced maximum at a low frequency $w \leqslant 0.1$. The height of the maximum decreases, width increases, and position shifts to the higher h with w increase. At fixed $h = 10$ nm, the dependence of δR on d is monotonic for low frequencies $w \leqslant 0.1$. A diffuse maximum appears at $w = 0.3$. At fixed $h = 5$ nm the dependence of δR on l has a pronounced maximum at the low frequencies $w \leqslant 0.1$. Note that the revealed maximum and its properties' size dependence can be of great importance for optimization of GFeFET performance, especially for the application in nonvolatile memory devices of new generation, where large δR is needed.

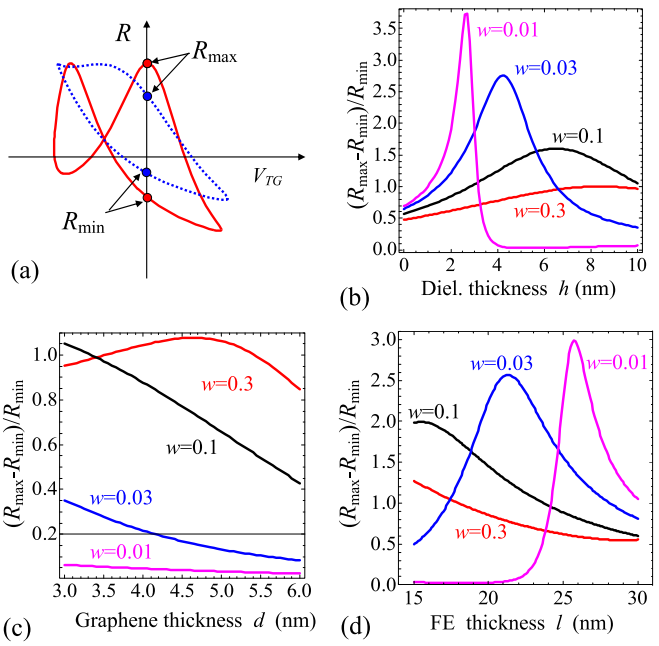

FIG. 4. (Color online) Size effect on graphene electroresistance. (a) Definition of the value $\delta R = (R_{\max} - R_{\min})/R_{\min}$ for resistance loops of different shape. (b)–(d) Dependences of δR on the dielectric layer, graphene, and ferroelectric film thicknesses h, d, and l calculated for different frequencies $w = 0.01-0.3$ (labels near the curves) are shown in the plots (b)–(d), correspondingly. Back gate voltage is $V_{BG} = 5$ V; top gate voltage amplitude is 30 V. Parameters for the plot (b): $R_t = 3$ nm, $d = 3$ nm, $l = 20$ nm; (c) $R_t = 3$ nm, $h = 10$ nm, $l = 20$ nm; (d) $R_t = 3$ nm, $h = 5$ nm, $d = 3$ nm. Other parameters are the same as in Fig. 2.

Figure 4 shows the dependence of the differential electroresistance, $\delta R = (R_{\max} - R_{\min})/R_{\min}$, on the thickness of

To summarize the modeling results presented in this section, first of all let us underline that the graphene-on-ferroelectric system demonstrates pronounced finite-size effects. Using this fact one can effectively control and optimize the nonlinear and hysteretic properties of the system by varying the thicknesses of the layers. Secondly, our theoretical approach is capable of describing available experimental results.

V. DOMAIN STRUCTURE IMPACT ON THE EQUILIBRIUM SPACE-CHARGE REDISTRIBUTION IN MLG

We further consider a ferroelectric film with domain stripes, whose domain walls are perpendicular to the film surface and to the transport direction along the graphene channel (see Fig. 1). The orientation of domain stripes is typical for thin ferroelectric films, especially for uniaxial ferroelectrics. External electric dragging field E_S is applied in the x direction between the source and drain electrodes located at graphene surface $z = -d$. In this case, one of the boundary conditions [see Eq. (2)] should be modified as $\varphi_G(x,y,z=-d) = V_{TG} - xE_S$. The stationary solution for electric potential in a multidomain state of ferroelectric is listed in the Appendix (also see Supplemental Material [24]). For the orientation the depolarization field induced by the stripes has maximal component directed along the dragging field E_S. The component is minimal (ideally absent) for the domain walls parallel to the film surface. Hence the chosen orientation of domain stripes corresponds to the maximal

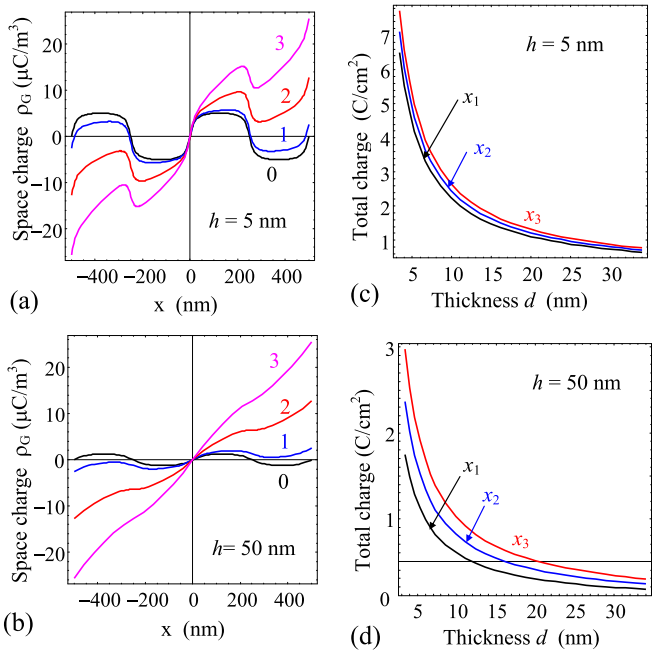

FIG. 5. (Color online) Effect of domain stripes. (a), (b) Space-charge x distribution at $z = -d + R_t/2 = -3.15$ nm caused in MLG by ferroelectric domain stripes in Rochelle salt, with the presence of sapphire layer of different thickness $h = 5$ nm and 50 nm on ferroelectric surface. Driving electric field $E_S = 0$, 10, 50, and 100 V/m (curves with labels 0, 1, 2, and 3, correspondingly), $V_{TG} = V_{BG} = 0$. Ferroelectric film thickness $l = 300$ nm, domain stripe period $a = 500$ nm, MLG thickness $d = 3.4$ nm ($N = 10$ graphene layers), multilayered graphene permittivity $\varepsilon_G = 15$ (graphite), Thomas-Fermi screening radius in graphene is $R_t = 0.5$ nm. (c), (d) Total charge dependence on MLG thickness d calculated at different x coordinates $x_1 = 125$ nm, $x_2 = 725$ nm, and $x_3 = 1125$ nm. The results are field dependent; here we put $E_S = 1$ kV/m.

impact of the domain structure on the transport properties of graphene.

Below we study the space-charge redistribution caused by domain stripes for the system "multilayered graphene–dielectric–ferroelectric thin film." A full set of parameters is listed in Table I. Complex size effects possibly appearing in the case of the domain stripe period $a \sim h$ will be considered elsewhere. Below we mainly use the value of 500 nm that is much higher than graphene and dielectric thickness. Applied fields $E_S = (0-10^3)$ V/m are typical for the graphene-on-ferroelectric devices [21].

According to a well-known electrostatic problem, the electric field caused by the periodic distribution of the surface charges with alternating signs exponentially vanishes with the distance from the surface. Thus when the period of the domain stripes a becomes comparable or smaller than the thickness of dielectric layer h, the influence of the depolarization field on the electric transport in graphene gradually decreases and practically disappears at $a \ll h$. The gradual decrease of the depolarization field leads to the transformation of the rectangularlike space-charge modulation in graphene to shallow harmonic modulation that vanishes in the limit $a \ll h$. When the period of domain stripes becomes much larger than h, the depolarization field in the central part of any stripe tends to the single-domain limit given by Eq. (4c) and the corresponding space-charge modulation acquires a pronounced rectangularlike profile.

Figures 5(a) and 5(b) illustrate the influence of applied field E_S and dielectric gap thickness on the space-charge-density distribution in the MLG modulated by the ferroelectric domain stripes. Within Thomas-Fermi or Debye approximations, the space-charge density is proportional to the electric potential, so their spatial modulations are in the antiphase. In the case of ultrathin dielectric layer ($h < 10$ nm) the potential and space-charge distributions are strongly affected by the depolarization field created by domains. In this case $h > 10$ nm and $0 < E_S < 50$ V/m, and the charge-density x profile is a quasiharmonic function with maxima in the center of the domains and zero values on the domain wall. The effect is manifested as quasirectangular modulation for $E_S = 0$ and there is a slightly inclined step for $0 < E_S < 500$ V/m. The steps becomes smoother and smaller with the h increase and almost disappear at $h = 50$ nm and $E_S > 50$ V/m indicating that for this case the external field effect appeared stronger than the depolarization field influence near the graphene upper surface $z = -d$. The event can be interpreted as a field-induced phase transition of the second order. Note that for E_S smaller than some critical value (<1 kV/m) there are p and n domains in MLG with electron and hole conductivity, correspondingly, and the dominant scattering mechanism thus can be due to the p-n junction at the domain walls (see [25] and references therein). For the higher fields there are no p and n domains, suggesting the change of the dominant scattering mechanism (e.g., towards scattering on the charged impurities, present in the dielectric layer [2] or on the interface, which is generally less intensive than the long-range disorder scattering, described in Ref. [23]) and the dramatic increase of the MLG channel conductivity. The effect can be used in applications of ferroelectric as sensors.

The total charge density calculated at [$E_S = 1$ kVm is shown in Figs. 5(c) and 5(d) for $h = 5$ and dielectric layer thickness $h = 50$ nm. Plots illustrate the monotonic decrease of the maximal total charge with graphene thickness increase, i.e., finite-size effect. Saturation appears with the d increase.

Finally we expect a rather strong orientation dependence of the transport properties on the domain stripes' direction with respect to the film surface. The effect can open the possibility of additional transport control in graphene by triggering the domain walls' orientation in multiaxial ferroelectric substrate. Unfortunately this interesting question is beyond the scope of the present study.

VI. CONCLUSION

We propose the combined self-consistent approach to describe graphene-on-ferroelectric dynamic behavior and obtained analytical results describing the finite-size effect in the system, which are necessary steps to transform the state-of-the-art from an empirical to an analytical level. Basic results obtained in this work are the following.

The main physical factor responsible for the resisting memory effect in the considered heterostructure "multilayer graphene–dielectric layer–ferroelectric film" is the hysteresis

of the internal depolarizing electric field, which appears in the dielectric layer between multilayer graphene and ferroelectric film. The depolarizing fields originated from the incomplete screening of ferroelectric film spontaneous polarization in the dielectric layer. Since the field reverses its sign under the spontaneous polarization reversal taking place when the external field exceeds the coercive one (ferroelectric hysteresis), the process causes nonlinear hysteretic dynamics of graphene charge and electroresistance.

The analytical expressions for the acting electric field, graphene charge, and electroresistance are derived in the case when a uniformly polarized ferroelectric film is a perfect insulator, and its surface is free of screening charges. As anticipated the field value is defined by the thicknesses of dielectric layer h, multilayer graphene film d, and ferroelectric film l. The analytical expressions helps us to reach a comprehensive understanding of the physical process, as well as to predict and to analyze multiscale finite-size effects in the system, which in turn opens an effective way to control and optimize its nonlinear and hysteretic properties. In particular, the versatile shape of the graphene charge and electroresistance hysteresis loops appears in the system depending on the thicknesses of the layers h, l, and d, and frequency and amplitude of electric voltage applied to the top gate (see Table II). Note that calculated resistance loops are very similar to the experimental ones obtained earlier by Zheng *et al.* [10] in GFeFET and correlate with the mechanism of the "direct" hysteresis of graphene channel resistivity, caused by repolarization of the dipoles in a ferroelectric substrate [23].

The approach proposed for a single-domain film can be further evolved for the description of the space-charge accumulation in the graphene-on-ferroelectric system allowing for the ferroelectric domain structure. In particular, when the ferroelectric substrate has evolved the stripe domain structure and a driving electric field E_S is applied along the graphene channel, the domain stripes of different polarity can induce domains with p and n conductivity in a multilayer graphene strip for E_S smaller then some critical value. Thus for the case the dominant carrier scattering mechanism can be randomly distributed p-n-junction potentials, whose position correlates with the domain walls in ferroelectric film. For the higher fields there are no pronounced p and n domains, and only smeared ripples remained, which indicates the change of the dominant scattering mechanism and the dramatic increase of the graphene channel conductivity. This intriguing effect can open possibilities for graphene-based sensors and explore the physical mechanisms underlying the operation of a graphene field-effect transistor with ferroelectric gating.

TABLE II. Finite-size effects.

Size	Influence on polarization P_3	Influence on total charge σ_G	Influence on electroresistance R and its variation $\delta R = (R_{\max} - R_{\min})/R_{\min}$
Dielectric layer thickness h	Remanent polarization decreases with increasing h	The total charge maximal difference (amplitude) decreases with increasing h.	Double peaks of resistance dependence get closer and become less "sharp" with h increase.
	Coercive voltages, as well as the maximal loop width, decrease with increasing h. The loops lose the squarelike and acquire slimlike shape with h increase.		$\delta R(h)$ has a pronounced maximum at low frequencies, whose height decreases, width increases, and position shifts to higher h values with frequency increase
Multilayer graphene thickness d	Remanent polarization decreases with increasing d	The total charge amplitude decreases with increasing d	The loops' asymmetry increases as d increasea and double shape loops transform into a single shape.
	Coercive voltages, as well as the maximal loop width, decrease with increasing d. For layers of graphite (more than 30 graphene layer) hysteresis loops are not revealed		
Ferroelectric thickness l	Remanent polarization values decrease with l decrease.	The total charge amplitude decreases with decreasing l.	The difference between two peaks of resistance increases with increasing l.
	Coercive voltage values decrease with l decrease.		$\delta R(l)$ has a maximum at low frequencies, whose height decreases, width increases, and position shifts to smaller l values with frequency increase
Screening radius R_t	Remanent polarization decreases with increasing R_t.	Total charge value becomes smaller with R_t increase.	Resistance loops' double shape transforms into a single one with R_t increase.
	Coercive voltage values decreases with increasing R_t; hysteresis loop almost disappears when multilayer graphene thickness d becomes more than $2R_t$. Loops become smoother with increasing R_t.		

ACKNOWLEDGMENTS

A.N.M., O.V.V., and E.A.E. acknowledge National Academy of Sciences of Ukraine, Grant No. 35-02-15, and Center for Nanophase Materials Sciences, User Projects No. CNMS 2013-293 and No. CNMS 2014-270. Research for S.V.K. was supported by the US Department of Energy, Basic Energy Sciences, Materials Sciences and Engineering Division. The authors are very grateful to Lisa A. Goins for helping with the manuscript preparation.

APPENDIX

The contributions of the top and bottom gate potentials V_{TG} and V_{BG} and polarization P_3 into the solution of the boundary problem (1)–(3) are given by these expressions:

$$\varphi_G(z) = \frac{\begin{pmatrix} V_{TG}\left\{e^{(d+z)/R_t}\varepsilon_d\varepsilon_G l(e^{-2z/R_t}+1)+\varepsilon_{33}^f[\varepsilon_G h(e^{-2z/R_t}+1)+\varepsilon_d R_t(e^{-2z/R_t}-1)]\right\} \\ +\varepsilon_d R_t\left[\varepsilon_{33}^f V_{BG}-(P_3 l/\varepsilon_0)\right](e^{(2d+z)/R_t}-e^{-z/R_t}) \end{pmatrix}}{\varepsilon_d\varepsilon_G l(e^{2d/R_t}+1)+\varepsilon_{33}^f[\varepsilon_G h(e^{2d/R_t}+1)+\varepsilon_d R_t(e^{2d/R_t}-1)]}, \tag{A1a}$$

$$\varphi_d(z) = \frac{2V_{TG}e^{d/R_t}\left[\varepsilon_d l+\varepsilon_{33}^f(h-z)\right]\varepsilon_G+\left[\varepsilon_{33}^f V_{BG}-(P_3 l/\varepsilon_0)\right][\varepsilon_d R_t(e^{2d/R_t}-1)+\varepsilon_G z(e^{2d/R_t}+1)]}{\varepsilon_d\varepsilon_G l(e^{2d/R_t}+1)+\varepsilon_{33}^f[\varepsilon_G h(e^{2d/R_t}+1)+\varepsilon_d R_t(e^{2d/R_t}-1)]}, \tag{A1b}$$

$$\varphi_f(z) = V_{BG}+(h+l-z)\frac{\varepsilon_d\varepsilon_G[2V_{TG}e^{d/R_t}-V_{BG}(e^{2d/R_t}+1)]-[\varepsilon_G h(e^{2d/R_t}+1)+\varepsilon_d R_t(e^{2d/R_t}-1)](P_3/\varepsilon_0)}{\varepsilon_d\varepsilon_G l(e^{2d/R_t}+1)+\varepsilon_{33}^f[\varepsilon_G h(e^{2d/R_t}+1)+\varepsilon_d R_t(e^{2d/R_t}-1)]}, \tag{A1c}$$

where the subscript $j = G,\ d,\ f$ means graphene, dielectric, and ferroelectric correspondingly.

Using a screening radius approximation, Eq. (1) (see also [4]), the space-charge density $\rho_G(z)$ in the multilayered graphene is given by the expression $\rho_G(z) = -\varepsilon_0\varepsilon_G\frac{\varphi_G(z)}{R_t^2}$. The total charge σ_G is the sum of the thickness space-charge density $\rho_G(z)$ integrated over graphene and the surface charge are determined by the boundary condition at the graphene-top gate interface, $z = -d$, as $D_3^G(-d) = \sigma_S$. In accordance with the principle of the whole system electroneutrality, the total charge stored in graphene is opposite in sign to the electric displacement at the bottom electrode, $D_3^f|_{z=L} = (\varepsilon_0\varepsilon_{33}^f E_3^f + P_3)|_{z=L}$, that in allowance for Eq. (4) gives Eq. (5). See Table II.

[1] K. S. Novoselov, A. K. Geim, S. V. Morozov, D. Jiang, M. I. Katsnelson, I. V. Grigorieva, S. V. Dubonos, and A. A. Firsov, Nature **438**, 197 (2005).

[2] A. Geim, Science **324**, 1530 (2009).

[3] K. Novoselov, A. Geim, S. Morozov, D. Jiang, Y. Zhang, S. Dubonos, I. Grigorieva, and A. Firsov, Science **306**, 666 (2004).

[4] S. Das Sarma, S. Adam, E. H. Hwang, and E. Rossi, Rev. Mod. Phys. **83**, 407 (2011).

[5] N. M. R. Peres, Rev. Mod. Phys. **82**, 2673 (2010).

[6] S. Kim, J. Nah, I. Jo, D. Shahrjerdi, L. Colombo, Z. Yao, E. Tutuc, and S. K. Banerjee, Appl. Phys. Lett. **94**, 062107 (2009).

[7] A. Konar, T. Fang, and D. Jena, Phys. Rev. B **82**, 115452 (2010).

[8] Y. Zheng, G.-X. Ni, C.-T. Toh, M.-G. Zeng, S.-T. Chen, K. Yao, and B. Özyilmaz, Appl. Phys. Lett. **94**, 163505 (2009).

[9] X. Hong, J. Hoffman, A. Posadas, K. Zou, C. H. Ahn, and J. Zhu, Appl. Phys. Lett. **97**, 033114 (2010).

[10] Y. Zheng, G.-X. Ni, C.-T. Toh, C.-Y. Tan, K. Yao, and B. Özyilmaz, Phys. Rev. Lett. **105**, 166602 (2010).

[11] Y. Zheng, G.-X. Ni, S. Bae, C.-X. Cong, O. Kahya, C.-T. Toh, H. R. Kim, D. Im, T. Yu, J. H. Ahn, B. H. Hong, and B. Özyilmaz, Europhys. Lett. **93**, 17002 (2011).

[12] E B. Song, B. Lian, S. M. Kim, S. Lee, T.-K Chung, M. Wang, C. Zeng, G. Xu, K. Wong, Y. Zhou, H. I. Rasool, D. H. Seo, H.-J. Chung, J Heo, S. Seo, and K. L. Wang, Appl. Phys. Lett. **99**, 042109 (2011).

[13] G-X. Ni, Y. Zheng, S. Bae, C. Y. Tan, O. Kahya, J. Wu, B. H. Hong, K. Yao, and B. Özyilmaz, ACS Nano **6**, 3935 (2012).

[14] S. Raghavan, I. Stolichnov, N. Setter, J.-S. Heron, M. Tosun, and A. Kis, Appl. Phys. Lett. **100**, 023507 (2012).

[15] M. Humed Yusuf, B. Nielsen, M. Dawber, and X. Du, Nano Lett. **14**, 5437 (2014).

[16] A. N. Morozovska and M. V. Strikha, J. Appl. Phys. **114**, 014101 (2013).

[17] A. N. Morozovska, E. A. Eliseev, A. V. Ievlev, O. V. Varenyk, A. S. Pusenkova, Y.-H. Chu, V. Ya. Shur, M. V. Strikha, and S. V. Kalinin, J. Appl. Phys. **116**, 066817 (2014).

[18] M. V. Strikha, J. Phys. Opt. **12**, 162 (2011).

[19] X. Hong, K. Zou, A. M. DaSilva, C. H. Ahn, and J. Zhu, Solid State Commun. **152**, 1365 (2012).

[20] M. V. Strikha, Ukr. J. Phys. Opt. **13**, S5 (2012).

[21] M. V. Strikha, Non-volatile memory of new generation and ultrafast IR modulators based on graphene on ferroelectric Substrate, in *Functional Nanomaterials and Devices for Electronics, Sensors and Energy Harvesting*, edited by A. Nazarov, F. Balestra, V. Kilchytska, and D. Flandre (Springer International Publishing, Switzerland, 2014), pp. 163–179.

[22] N. W. Ashcroft and N. D. Mermin, *Solid State Physics* (Thomson Learning, Toronto, 1976).

[23] A. I. Kurchak, A. N. Morozovska, and M. V. Strikha, Ukr. J. Phys. **58**, 472 (2013).

[24] See Supplemental Material at http://link.aps.org/supplemental/10.1103/PhysRevB.91.235312 for the Stationary solution for electric potential in a multidomain state of ferroelectric.

[25] A. I. Kurchak and M. V. Strikha, Ukr. J. Phys. **59**, 622 (2014).